Available online at www.sciencedirect.com
ScienceDirect
Vibrational Spectroscopy 44 (2007) 357–368
VIBRATIONAL SPECTROSCOPY
www.elsevier.com/locate/vibspec

Density functional theory based calculations of the vibrational properties of chlorophyll-*a*

Ruili Wang, Sreeja Parameswaran, Gary Hastings *

Department of Physics and Astronomy, Georgia State University, 29 Peachtree Center Avenue, Atlanta, GA 30303, United States

Received 29 November 2006; received in revised form 8 March 2007; accepted 13 March 2007
Available online 23 March 2007

Abstract

Chlorophyll-*a* plays a fundamental role in the solar energy conversion processes that occur in oxygen evolving organisms, such as plants algae and cyanobacteria. To study the chlorophyll-*a* species at the heart of these solar conversion processes FTIR difference spectroscopy has been a valuable tool. However, FTIR difference spectra are only partially understood. To gain a more detailed understanding of FTIR difference spectra one of our goals is to calculate the vibrational properties of the chlorophyll-*a* systems found in plants and bacteria, and compare this to the properties found for isolated chlorophyll molecules in the gas phase and in solvents. As a first approach to this problem, we have calculated the vibrational properties of several chlorophyll-*a* model molecular systems using hybrid density functional theory at the B3LYP/6-31G(d) level. In particular, attention is focused on the infrared active vibrational modes of the carbonyl groups of chlorophyll-*a*, since these are the species that give rise to intense bands in infrared absorbance and absorbance difference spectra. The different chlorophyll-*a* models studied differ only in the number of carbonyl groups included in the model. In this way, it is possible to asses how the different C=O modes couple. This is an important goal for a detailed understanding of the FTIR difference spectra. It also provides a very stringent test of the applicability of various computational approaches. Knowledge of how the different C=O modes in monomeric chlorophyll species couple is also an important prerequisite for studies of multimeric or aggregated chlorophyll species, because in these aggregated species the carbonyl groups of the chlorophylls provide axial ligands to other chlorophylls.

The infrared absorbance spectra and ''cation minus neutral'' infrared absorbance difference spectra of a model chlorophyll-*a* molecular system that contains the 13^1-keto carbonyl group and the 17^3-ester carbonyl group are calculated. The calculated spectra agree well with the corresponding experimentally determined spectra for pyrochlorophyll-*a* in polar solvents.

When the vibrational properties of model chlorophyll-*a* molecular systems that contain both the 13^1-keto and 13^3-ester carbonyl group are calculated it is found that there is a strong coupling between the two carbonyl modes for the neutral species. In addition, for the chlorophyll-*a* cation, it is found that the calculated 13^1-keto carbonyl mode frequency is higher than that of the 13^3-ester carbonyl mode (although the two modes are no longer coupled). These calculated results do not agree with experiment. At the computationally more expensive 6-31+G(d) level, the calculations did give a more accurate description of the C=O modes of neutral chlorophyll-*a*. However, there was still a considerable coupling between the 13^1-keto and 13^3-ester carbonyl modes. Calculations at the 6-31G(d) level do provide an accurate description of the experimentally determined behavior of the C=C modes of chlorophyll-*a*, however.

Finally, infrared absorbance spectra were calculated for chlorophyll-*a* model molecular systems that were fully ^2H, ^{15}N and ^{13}C labeled. In spite of the complicated coupling between the 13^1-keto and 13^3-ester carbonyl modes, it is found that calculated isotope induced vibrational frequency band shifts do closely match experiment.

The calculations described here form a foundation on which to base more detailed calculations of chlorophylls in solvent or protein environments, or calculations of multimeric chlorophyll species. Such calculations will be undertaken as computational power increases.

Keywords: Chlorophyll-*a*; Density functional theory; Fourier transform infrared; Normal mode; Vibrational frequencies

1. Introduction

Chlorophylls (Chls) play a fundamental role in both prokaryotic and eukaryotic photosynthesis. They are the molecular species that are responsible for both light energy

Abbreviations: Chl-*a*, chlorophyll-*a*; C=O, carbonyl; DFT, density functional theory; DS, difference spectrum, spectra, spectroscopic or spectroscopy; FTIR, Fourier transform infrared; H, hydrogen atom; IR, infrared; pChl-*a*, pyrochlorophyll-*a*; THF, tetrahydrofuran

* Corresponding author. Tel.: +1 404 651 0748; fax: +1 404 651 1427.
E-mail address: ghastings@gsu.edu (G. Hastings).

0924-2031/$ – see front matter © 2007 Elsevier B.V. All rights reserved.
doi:10.1016/j.vibspec.2007.03.005

capture and its conversion into an electrochemical gradient [1]. In photosynthetic oxygen evolving organisms, such as plants and cyanobacteria, two photosystems called photosystem I and photosystem II (PS I and PS II) capture and convert solar energy independently (but cooperatively) [2]. PS II uses light to catalyze the oxidation of water, with the subsequent liberation of molecular oxygen [3,4]. The solar conversion processes in PS II are responsible for the earth's oxygen rich atmosphere. PS I uses light to catalyze the formation of products that are ultimately used to reduce carbon dioxide, leading to its incorporation into larger complex organic molecules (glucose). In both PS I and PS II, the molecular species at the heart of all of the solar capture and conversion processes is chlorophyll-*a* (Chl-*a*).

The primary photochemical event in all photosynthetic organisms is the excitation of a chlorophyll (Chl) species and the subsequent transfer of an electron to a nearby acceptor (which is also usually a Chl species). In PS I and PS II the primary donors are dimeric Chl-*a* species called P680 and P700, respectively [3].[1] P680 and P700 have widely varying redox properties, and it is these properties that lie at the heart of the differing functions of PS I and PS II [3].

Given the widespread use of Chls in all photosynthetic organisms, and in particular the use of Chl-*a* in oxygenic photosynthesis, one goal of photosynthesis research is the development of a quantitative understanding of Chl-*a* and its various types of aggregated forms that act as electron donors. Unfortunately, a fully quantum mechanical calculation of the thermodynamic properties of aggregated Chls (in a protein matrix) is not likely in the near future, due to limitations in computational power. However, it is now computationally feasible to calculate (quantum mechanically) some of the properties of isolated Chl molecules in both the neutral and radical form. Such calculations are a prerequisite, not only for future calculations on naturally occurring aggregated Chl systems, but also for the theoretical study of isolated or aggregated Chl molecules that can be bound to surfaces or other molecules in artificial solar converting constructs.

Primary electron donors in several types of photosynthetic particles have been widely studied using FTIR difference spectroscopy (DS) [5–7]. Such a technique provides information on the vibrational properties of both the neutral and cationic species. Chl in various organic solvents have also been studied using FTIR DS [8,9]. The frequency and intensity information available in these difference spectra provides a wealth of information on the hydrogen bonding status as well as on the polarity of the environment of specific functional groups that are part of the molecule. However, given the complexity of *in vivo* pigment–protein systems, assignment of FTIR bands to vibrational modes in specific types of environments is very difficult. There is a demonstrated need for a quantitative understanding of how vibrational mode frequencies and intensities change upon radical formation, and upon changes in environment (introduced through for example, site directed mutagenesis). Our initial approach, outlined below, is to compare experimental results on isolated Chl molecules in solvent with theoretical gas-phase calculation. If a direct connection between theory and experiment can be established then this will set a firm foundation for studies on more complex systems. In addition, it will be possible to use the calculations as a tool to predict how the vibrational properties of a system may be modified following some type of perturbation. The predictions derived can then be tested experimentally. In this way, a quantitative understanding of Chl molecules in protein environments may be developed. This is likely to be a reachable goal given the continuing increases in computational power that are occurring, and the development of more efficient quantum chemical algorithms.

As mentioned above, Chl-*a* is the major pigment found in all oxygenic photosynthetic organisms. The molecular structure of Chl-*a* is shown in Fig. 1. It contains three carbonyl (C=O) groups at the 13^1, 13^3 and 17^3 positions. The three C=O groups have large dipole moments and give intense infrared (IR) absorbance bands [10].

Some calculations of the properties of Chl-*a* have been undertaken previously. The hyperfine coupling constants as well as the spin density distribution of Chl-a^+ were calculated using semi-empirical (RHF/INDO/SP) and density functional (at the BLYP/DZVP [11] and B3LYP/EPR-II SP levels [12]) methods. More recently, the influence of axial Mg^{2+} ligation and peripheral hydrogen bonding (H-bonding) on the on the electronic orbitals of Chl-*a* were investigated using density functional theory (DFT) at the B3LYP/6-31G(d) level [13]. Ceccarelli et al. [14] performed normal mode vibrational frequency calculations for neutral methylbacteriochlorophyllide-*a* using DFT in the local density plus gradient correlation

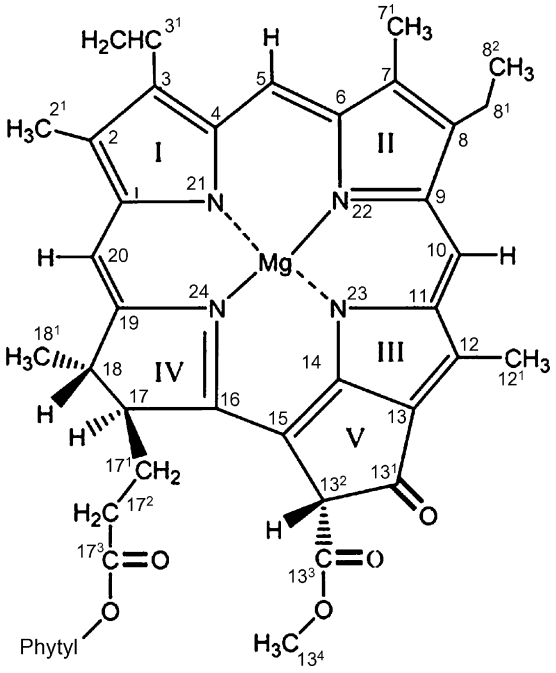

Fig. 1. Molecular structure and IUPAC numbering scheme of Chl-*a*.

[1] It has been suggested that the primary donor in both PS I and PS II are monomeric Chl species, and that the familiar dimeric Chl species are oxidized by this primary donor [26].

approximation. Only in plane vibrations were discussed, however. Berezin and coworkers used DFT methods (B3LYP/6-31G(d) level) to calculate the normal mode vibrational frequencies of neutral ethylbacteriochlorophyllide-*a* [15] and neutral ethylchlorophyllide-*a* [16]. These latter calculations concentrated only on the neutral species, so available FTIR difference spectra could not be used to help assess the accuracy of their calculations. One goal of this manuscript is to investigate the vibrational properties of Chl-a^+, with the goal of calculating a "Chl-a^+ minus Chl-*a*" infrared difference spectrum (IR DS) that can be compared directly to corresponding spectra generated electrochemically. In this manuscript, we focus on calculations of IR spectra for molecules in the gas phase. However, we showed previously that such calculations can be very usefully compared to experimental FTIR spectra of molecules in solvent [17].

FTIR DS of biological molecules in combination with isotope labeling studies is a useful approach for associating molecular modes with FTIR difference bands. In large biomolecules, however, many of the modes are coupled and the isotope induced band shifts as well as band intensity changes expected are far from certain. Isotope induced band frequency and band intensity changes can be calculated for all vibrational modes, however. These calculated shifts can then be directly compared with experiment and band assignments can be made accordingly. The combination of FTIR DS with isotope labeling, with inclusion of vibrational frequency calculations, is therefore of considerably greater utility.

Recently, O'Malley has used DFT to calculate the vibrational properties of a Chl-*a* model that contains the 13^1-keto C=O group but lacks the 13^3 and 17^3-ester C=O groups [12]. Only three normal modes for the neutral and cationic species were presented, however. Although the single C=O containing Chl-*a* model can account for many of the magnetic properties of Chl-*a*, it is obviously insufficient for comparison with experimental IR data. However, the calculations of O'Malley serve as a useful starting point from which to develop our computational studies in a systematic fashion.

In the computational studies reported here, we extend the calculations undertaken on the simplest Chl-*a* model system by O'Malley (denoted Chl-a_1). First we present the complete set of calculated normal mode vibrational frequencies and intensities for Chl-a_1 (only three of the 132 frequencies were published previously). We then present calculated "cation minus neutral" IR DS for Chl-a_1 and compare it to experimental IR spectra obtained for pyrochlorophyll-*a* (pChl-*a*) in THF. We then undertake calculations using more realistic Chl-*a* models that contain two or all three of the C=O groups. Finally, we compute "cation minus neutral" IR DS for all of the Chl-*a* models when they are deuterated, ^{13}C and ^{15}N labeled. We compare computed isotope induced band shifts and intensity changes with available experimental data.

2. Experimental methods

All geometry optimizations and harmonic vibrational mode frequency calculations were performed using Gaussian 03 [18] (Gaussian Inc. Wallingford, CT). Unless stated, the B3LYP functional was used in combination with the 6-31G(d) basis set. At this level of theory, computed harmonic vibrational mode frequencies overestimate experimental anharmonic frequencies by approximately 5% [19]. Radical induced frequency shifts and isotope induced frequency shifts are accurately calculated, however [17]. Unless specified, no negative frequencies were calculated for any of the molecular structures discussed here.

3. Results and discussion

Fig. 1 shows the molecular structure of Chl-*a* along with the IUPAC numbering scheme. The IUPAC numbering scheme will be used throughout this manuscript. Here, the calculated vibrational properties of several model Chl-*a* molecules will be presented. The first, which we call Chl-a_1, contains only the 13^1-keto C=O group attached at ring V (Fig. 2A). Chl-a_1 contains the vinyl group at C_3 but all other substituents of the tetrapyrrole ring are replaced with hydrogen (H) atoms. Chl-a_1 was constructed directly using the software GaussView03. Chl-a_1 contains 46 atoms ($C_{24}H_{16}MgN_4O$), and is the same as the Chl-*a* model studied by O'Malley [12].

To investigate possible effects due to coupling of the C=O groups, we have studied a second Chl-*a* model, called Chl-a_2, that contains the 13^1-keto C=O group as well as the 17^3-ester C=O group, but lacks the 13^3-ester C=O group (Fig. 2B). Pyrochlorophyll-*a* (pChl-*a*) lacks the 13^3-ester C=O group but contains the 13^1-keto and the 17^3-ester C=O groups. Chl-a_2 is therefore a model for pChl-*a*. The third Chl-*a* model studied, Chl-a_3 (Fig. 2C), contains the 13^1-keto as well as the 13^3-ester C=O groups, but lacks the 17^3-ester C=O group (Fig. 2C). Chl-a_3 allows a study of the coupling between the 13^1-keto and the 13^3-ester C=O groups, without interference from the 17^3-ester C=O group. Finally, Chl-a_4 (Fig. 2D) contains the 13^1-keto C=O, as well as the 13^3 and 17^3-ester C=O groups. For Chl-a_3 and Chl-a_4 the 13^3-ester C=O group points out of the macrocycle plane and away from the 13^1-keto C=O group. The complete Guassian files for all of the models are available upon request. Selected bond lengths calculated for neutral and cationic Chl-a_1, Chl-a_2 and Chl-a_3 are presented in Supplementary information 1. For Chl-a_1 and Chl-a_1^+ the calculated bond lengths are identical to that calculated previously [12]. Most of the calculated bond lengths change upon cation formation. For example, for Chl-a_1/Chl-a_2/Chl-a_3 the 13^1-keto C=O bond decreases 0.008/0.007/0.007 Å upon cation formation, respectively (see Supplementary information 1).

3.1. Calculation of the vibrational properties of Chl-a_1 and Chl-a_2

Chl-a_1 and Chl-a_2 display 132 and 168 normal modes of vibration, respectively. Most of these modes have very low intensity and are undetectable in an FTIR absorbance spectrum. For this reason, we will usually discuss only the most intense vibrational modes. Calculated harmonic vibrational mode frequencies and intensities (in parenthesis) for the most prominent modes of Chl-a_1/Chl-a_2 and Chl-a_1^+/Chl-a_2^+ are

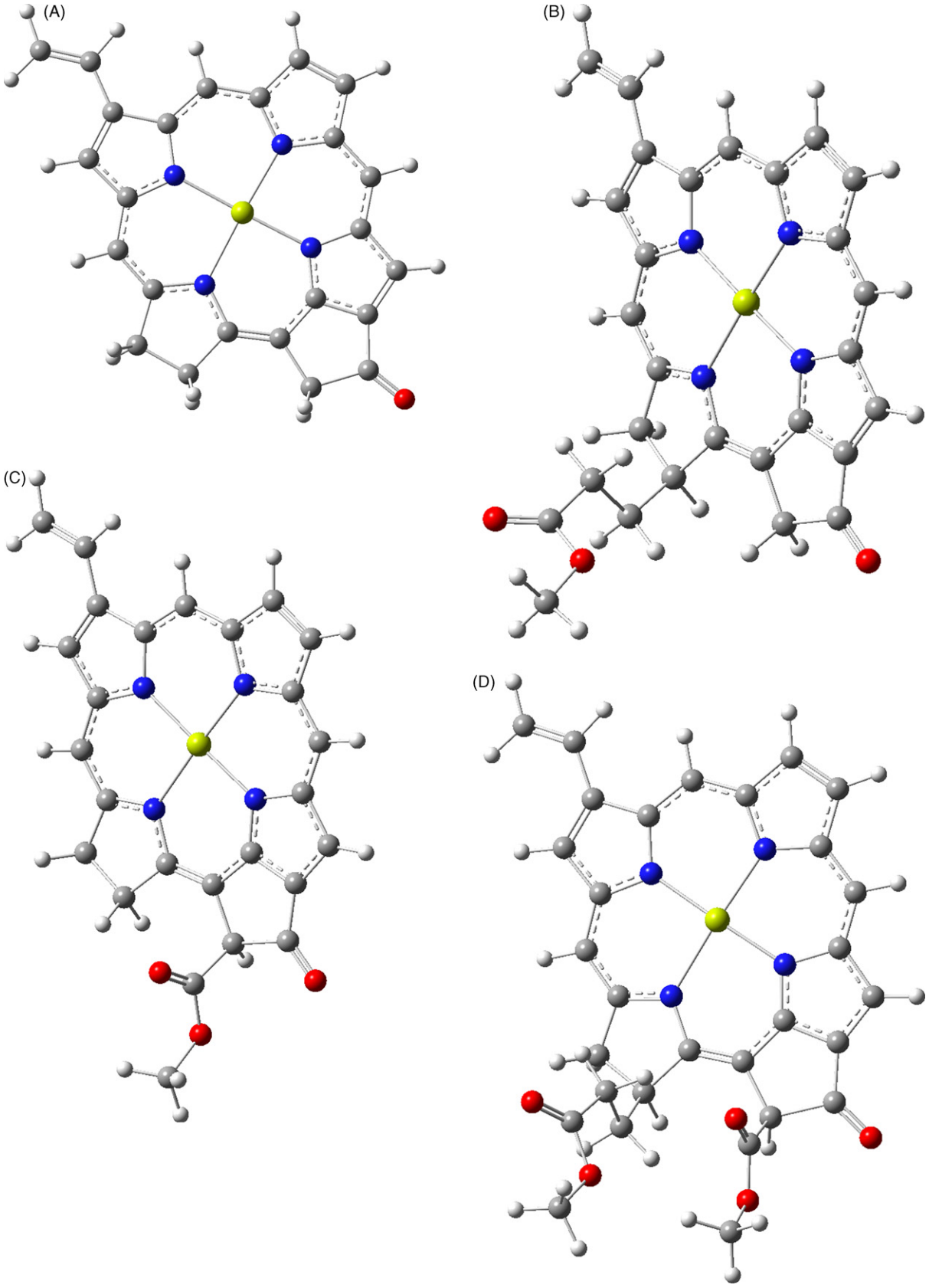

Fig. 2. Geometry optimized (energy minimized) molecular structure of (A) Chl-a_1, (B) Chl-a_2, (C) Chl-a_3 and (D) Chl-a_4. The structures were optimized using the B3LYP/6-31G(d) method.

Table 1
Prominent harmonic vibrational mode frequencies and intensities (in parenthesis) calculated for Chl-a_1, Chl-a_1^+, Chl-a_2 and Chl-a_2^+

Mode	Chl-a_1			Chl-a_2	
	Neutral ν(I)	Cation ν(I)	Cation II ν(I)	Neutral ν(I)	Cation ν(I)
$\nu(17^3$-ester C=O)				1830(231)	1839(210)
$\nu(13^1$-keto C=O)	**1806(717)**	**1832(424)**	1832(416)	1806(710)	1831(439)
ν(vinyl C=C)	**1701(3)**	**1684(63)**	1697(20)	1701(2)	1684(63)
$\nu(C_{15}=C_{16}, C_{19}=C_{20})$	**1660(264)**	**1639(320)**	1639(332)	1655(253)	1636(303)
$\nu(C_{12}=C_{13}, N_{23}=C_{14}, C_2=C_3)$, γ(C-H)	1593(158)	1582(435)	1584(327)	1590(219)	1582(371)
$\nu(C_5=C_6, C_{15}=C_{16})$		1568(398)	1569(396)		1566(484)
$\nu(C_{12}=C_{13})$, δ(C–H), γ(C–H)	1515(136)	1485(125)	1484(21)	1517(118)	1486(131)

Mode assignments are also listed. Frequencies are in cm^{-1} and intensities in km/mol. For the optimized Chl-a_1^+ geometry a negative frequency is calculated (see Supplementary information 2). Vibrational frequencies for an alternative Chl-a_1^+ geometry with the 3^1 vinyl pointing out of the macrocycle plane are also listed (labeled as cation II). Calculations were undertaken using the B3LYP method and the 6-31G(d) basis. Data shown in bold is virtually the same as that calculated previously [12]. Frequencies have not been scaled. *Abbreviations:* ν, δ, γ, stretching, bending and rocking.

presented in Table 1. Calculated normal mode frequencies and intensities for all modes of Chl-a_1, Chl-a_1^+, Chl-a_2 and Chl-a_2^+ are presented in Supplementary information 2.

Previously, O'Malley [12] presented only three of the calculated harmonic vibrational mode frequencies (and intensities) for Chl-a_1 and Chl-a_1^+. These data are shown in bold in Table 1. Advancing from that work, we present all of the vibrational frequencies and intensities of Chl-a_1 and Chl-a_1^+ (see Supplementary information 2). We also present all of the vibrational frequencies and intensities of Chl-a_2 and Chl-a_2^+, some of which are shown in Table 1.

From the calculated harmonic vibrational mode frequencies and intensities we are able to construct IR "stick" spectra. By convolving these stick spectra with a Gaussian function of 4 cm^{-1} bandwidth, more realistic looking IR spectra are obtained, which we will call absorbance spectra [20]. Fig. 3A shows calculated IR absorbance spectra for Chl-a_1 and Chl-a_1^+, as well as the corresponding "cation minus neutral" IR absorbance DS in the 1870–1200 cm^{-1} region (the spectra are presented at a density of one data point per centimeter). The corresponding spectra for Chl-a_2 are shown in Fig. 3B.

For Chl-a_1^+, one imaginary frequency is calculated (at -12 cm^{-1} with an intensity of 0.0461, see Supplementary information 2), indicating that the molecule studied is not the true energy minimized structure. We have found that it is not possible to calculate only real frequencies for Chl-a_1^+ (although we can for Chl-a_1) when the starting geometry has the 3^1 vinyl group lying in the plane of the macrocycle. By geometry optimizing Chl-a_1^+ starting from a molecule that has the vinyl group pointing out of the plane of the macrocycle we are able to calculate only real frequencies for Chl-a_1^+. In Fig. 3A, we show the spectrum calculated for geometry optimized Chl-a_1^+ with the vinyl group lying out of the macrocycle plane, characterized by a dihedral angle of $-147.5°$. The frequencies for this molecule are also listed in Table 1, labeled as cation II. The spectra for the two cation molecules with a differently oriented 3^1 vinyl group are very similar, and it is not entirely clear how much of a problem the calculation of only one or a few negative frequencies for a non optimized structure actually is. Certainly, the band at 1684 cm^{-1} is greatly modified when the vinyl group lies out of the macrocycle plane. This band is due to the vinyl C=C stretching vibration (Table 2) and will be of considerable relevance in calculations of Chl-a^+ Raman spectra.

Methods for assigning calculated vibrational frequencies to molecular groups are somewhat subjective, and have been

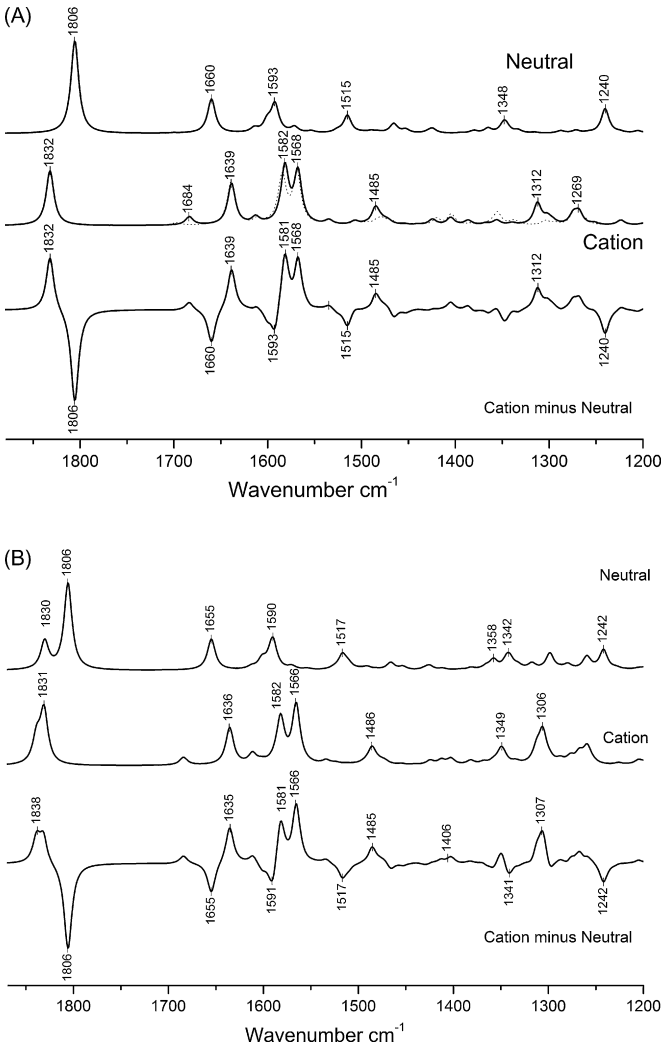

Fig. 3. Calculated IR absorption spectra for (A) Chl-a_1 and (B) Chl-a_2 in the gas phase. The neutral (top), cation (middle) and "cation minus neutral" (bottom) IR spectra are shown.

Table 2
Summary of calculated (Chl-a_1 and Chl-a_2) and experimentally observed (Chl-*a* and pChl-*a*) cation induced frequency shifts of the 13^1-keto C=O, 17^3-ester C=O and C=C modes

	Cation induced frequency up-shift 13^1-keto	Cation induced intensity decrease (%) 13^1-keto	Cation induced frequency up-shift 17^3-ester	Cation induced intensity decrease (%) 17^3-ester	I(17^3)/ I(13^3) %	Cation induced frequency downshift C=C	Cation induced intensity decrease (%) C=C
Calculated							
Chl-a_1	26	−41	–	–	–	21	21
Chl-a_2	25	−38	9	9	33	19	20
Experiment							
pChl-*a*	26[a]	∼−40[a]	–	–	33[b]		<10[b]
Chl-*a*	25[a]	∼−40[a]	–		33–50[b]		<10[b]

Cation induced changes in intensity of the modes are listed, as is the ratio in the intensity of the 17^3-ester C=O band to the 13^1-keto C=O band for the neutral state.
[a] From reference [9].
[b] From references [9,10].

described previously [20]. Vibrational mode frequencies are assigned by visual inspection, and only the molecular groups that most prominently contribute to the vibration are listed. Calculated normal mode frequencies presented here are unscaled, as no single scaling factor is satisfactory for all frequencies [21]. In addition, we are primarily interested in vibrational frequency changes that occur upon isotope labeling, or upon radical cation formation. Such frequency differences are accurately calculated without scaling [17], presumably because the same errors are inherent in calculation of the vibrational mode frequencies for both the labeled and unlabeled species, and/or the neutral and cation species. Normal mode intensities are also presented here, which has not been the case in many previous harmonic vibrational frequency calculations of Chl-*a* [12,16]. It is only with the frequency and intensity information that IR absorption spectra and difference spectra can be constructed and compared usefully to experimental data [17].

The most prominent band in the calculated IR absorbance spectrum of Chl-a_1 and Chl-a_1^+ is the 13^1-keto C=O mode. This mode occurs at 1806 cm^{-1} and up-shifts 26 cm^{-1} to 1832 cm^{-1} upon cation formation (Table 1, Fig. 3A). The 13^1-keto C=O mode also decreases in intensity by ∼41% upon cation formation [717 to 424 km/mol (Table 1)]. For neutral Chl-a_2 the 13^1-keto C=O mode occurs at 1806 cm^{-1} and up-shifts 25 cm^{-1} to 1831 cm^{-1} upon cation formation. The intensity of the mode also decreases by ∼38% upon cation formation [710 to 439 km/mol (Table 1)]. Clearly, the band frequency, intensity, and cation induced frequency shift of the 13^1-keto C=O mode are virtually the same for both Chl-a_1 and Chl-a_2 (Table 2), indicating that the 17^3-ester C=O group has virtually no impact on the vibrational properties of the 13^1-keto C=O group.

3.2. Comparison of the calculated vibrational properties of Chl-a_1 and Chl-a_2 with experiment

For Chl-a_2 the 17^3-ester C=O mode occurs at 1830 cm^{-1} and up-shifts 9 cm^{-1} upon cation formation. It also decreases in intensity by 9% (Fig. 3B and Table 2). For neutral Chl-a_2, the 17^3-ester C=O mode intensity is about three times less than that found for the 13^1-keto C=O mode (Table 2). These calculated properties of the 17^3-ester and 13^1-keto C=O groups can be usefully compared to experimental IR absorbance spectra (Fig. 9C in reference [10]) and "cation minus neutral" FTIR DS for pChl-*a* in tetrahydrofuran[2] (Fig. 2b and Table 2 in reference [9]).

From experimental IR absorption spectra of pChl-*a* in THF [10] the 13^1-keto C=O mode is found at 1688 cm^{-1} while the 17^3-ester C=O mode is found at 1737 cm^{-1} [10]. The difference in mode frequency between the two C=O modes is 49 cm^{-1}. For Chl-*a* in THF the observed difference is 40 cm^{-1} [9,10]. The calculated difference between the two C=O mode frequencies is only 24–25 cm^{-1} (Table 1). The calculations therefore poorly model this aspect of the experimental data.

Experimentally, for pChl-*a* in THF, the 17^3-ester C=O band is found to be about a factor of three less intense than the 13^1-keto C=O band [10]. We also calculate the 17^3-ester C=O mode to be a factor of ∼3 lower in intensity than the 13^1-keto C=O mode (Fig. 3B; Table 1). In this respect, the calculations agree well with experimental data.

From electrochemically generated (pChl-a^+ minus pChl-*a*) FTIR DS [9] an intense negative band is found at 1686 cm^{-1}, that up-shifts 26 cm^{-1} to 1712 cm^{-1} upon cation formation, and is due to the 13^1-keto C=O mode. The 17^3-ester C=O group appears to make only a very small contribution to (pChl-a^+-pChl-*a*) FTIR DS [9]. In contrast, our calculations predict a 9 cm^{-1} cation induced up-shift of the 17^3-ester C=O mode (Table 2). Such an up-shift should be clearly observable experimentally. Since this is not observed it would appear that our calculations do not accurately simulate this aspect of the experimental data. It may be the case that in solvents the 17^3-ester C=O group is more isolated from the charge distribution of the macrocycle. Table 2 summarizes the similarities and differences between the calculated data for Chl-a_1 and Chl-a_2

[2] In a polar solvent, such as THF, Chl-*a* exists in a disaggregated monomeric form, which is not the case for non-polar solvents, such as CCl_4. We therefore generally compare calculated data for Chl-*a* to spectra that were obtained in polar solvents.

with experimental absorption and absorption difference spectra of Chl-*a* and pChl-*a* in THF.

For Chl-a_1, the second most intense band in the calculated spectrum occurs at 1660 cm^{-1}. This band is predominantly due to C_{15}=C_{16} and C_{19}=C_{20} stretching vibrations. Several other C=C modes also weakly contribute to this band. The 1660 cm^{-1} band downshifts 21 cm^{-1} to 1639 cm^{-1} upon cation formation, and it increases in intensity by ~20% (Fig. 3A and Table 2). For neutral Chl-a_2, the corresponding mode is at 1655 cm^{-1}, and it displays virtually identical cation induced behavior as that found for Chl-a_1 (Fig. 3B). For neutral Chl-a_1 and Chl-a_2, the ~1655–1660 cm^{-1} C=C mode intensity is about three times less than that found for the 13^1-keto C=O mode (Table 1).

The calculated band at 1655–1660 cm^{-1} probably corresponds to the band observed at 1597–1620 cm^{-1} in IR spectra of most chlorophyll systems [10]. From the IR spectra of Chl-*a* in THF a C=C band is found at 1608 cm^{-1} and has an intensity that is 20–25% of that of the 13^1-keto C=O band [10]. Such an intensity ratio agrees well with our calculations.

Based on the above comparison between experimental and calculated IR absorbance spectra, our calculations predict the presence of a negative band in the 1620–1597 cm^{-1} region in both (Chl-a^+ minus Chl-*a*) and (pChl-a^+ minus pChl-*a*) FTIR DS, and a positive band ~21 cm^{-1} lower in frequency, with slightly increased intensity. In (Chl-a^+ minus Chl-*a*) and (pChl-a^+ minus pChl-*a*) FTIR DS negative band is observed at ~1597 cm^{-1}, that appears to downshift to 1585–1572 cm^{-1} upon cation formation, and increase slightly in intensity. Raman spectra of Chl-*a* and Chl-a^+ suggest that the cation induced downshift of C=C modes is less than 10 cm^{-1} [22,23]. Based on this, it is probably the case that the negative band near 1597 cm^{-1} in (Chl-a^+ minus Chl-*a*) and (pChl-a^+ minus pChl-*a*) FTIR DS downshifts ~12 cm^{-1} to 1585 cm^{-1}, which agrees well with our calculated downshift of ~20 cm^{-1}. Our calculated data (Table 2) therefore suggest that the observed negative difference band at ~1597 cm^{-1} is due to C_{15}=C_{16} and C_{19}=C_{20} stretching vibrations, which downshifts 12 cm^{-1} upon cation formation. In the (Chl-a^+ minus Chl-*a*) and (pChl-a^+ minus pChl-*a*) FTIR DS several positive features are observed between 1585 and 1572 cm^{-1} [9]. The calculated spectra in Fig. 3 suggest how such positive absorption features might occur. For Chl-a_1^+ and Chl-a_2^+ an intense band is found at 1568 cm^{-1}, which appears to have no counterpart in the spectra for the neutral species. The 1568 cm^{-1} band is due predominantly to C_5=C_6 and C_{15}=C_{16} stretching vibrations that are IR inactive in the neutral state. We propose therefore that the positive 1568 cm^{-1} band in the calculated cation spectra corresponds to part of the positive band in the 1570–1580 cm^{-1} region in the experimental (pChl-a^+ minus pChl-*a*) and (Chl-a^+ minus Chl-*a*) FTIR DS.

The calculated vinyl C=C stretching mode of Chl-a_1 occurs at 1701 cm^{-1} and downshifts 17–1684 cm^{-1} upon Chl-a_1^+ formation for the case in which the vinyl C=C lies in the plane of the macrocycle (for the case in which the vinyl C=C lies ~35° out of the plane the mode is found at 1697 cm^{-1}). This mode is virtually infrared inactive for the neutral state but increases in intensity by a factor of 21 upon cation formation (Table 1). The band associated with the vinyl C=C stretch is clearly visible in the spectrum of Chl-a_1^+ but it is still about seven times less intense than the band associated with the 13^1-keto C=O mode (Table 1).

3.3. Calculation of the vibrational properties of Chl-a_3

From electrochemically induced (Chl-a^+ minus Chl-*a*) and (pChl-a^+ minus pChl-*a*) FTIR DS it has been determined that removal of the 13^3-ester C=O group leads to a 6–7 cm^{-1} downshift of the 13^1-keto C=O mode frequency of Chl-*a* or Chl-a^+ [9]. The same results were found from IR absorbance spectra of neutral Chl-*a* and pChl-*a* [10]. This IR data indicates some coupling of the 13^1-keto and 13^3-ester C=O groups. To investigate computationally how the 13^3-ester C=O group couples to the 13^1-keto C=O group in the absence of the 17^3-ester C=O we have calculated the vibrational properties of the Chl-a_3 model shown in Fig. 2C. For Chl-a_3, the ester C=O group points out of the plane of the macrocycle, and slightly away from the 13^1-keto C=O group. The 3^1 vinyl C=C group lies in the plane of the macrocycle for both the neutral and cation species.

Chl-a_3 displays 150 normal modes of vibration. Again, most of these modes are undetectable in an IR absorbance spectrum. Fig. 4 shows calculated absorbance spectra for (A) Chl-a_3 and (B) Chl-a_3^+, in the 1870–1200 cm^{-1} region. The "cation minus neutral" IR DS is also shown in Fig. 4C. For the cation state no negative frequencies are calculated, even for the model shown in Fig. 2C with the vinyl group in the plane of the macrocycle. Table 3 lists several of the harmonic vibrational mode frequencies and intensities (in parenthesis) and their approximate mode assignments for Chl-a_3 and Chl-a_3^+.

For neutral Chl-a_3 the mode compositions are considerably more complex than for the previous two models. For neutral Chl-a_3 the 13^1-keto and 13^3-ester C=O mode vibrations cannot be distinguished. Instead, the modes at 1806/1817 cm^{-1} are

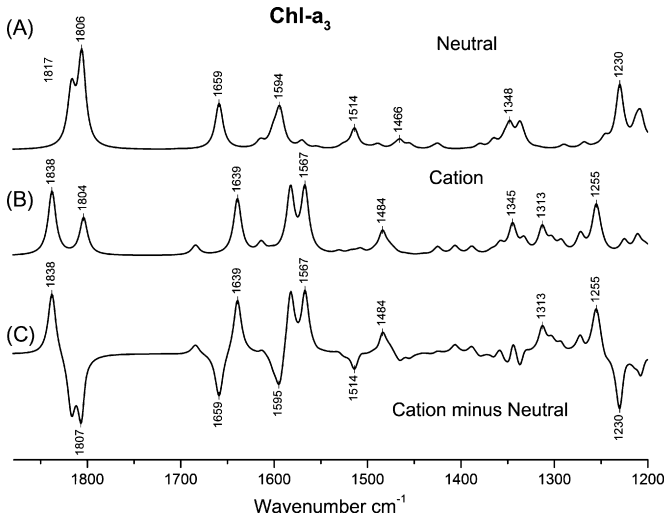

Fig. 4. Calculated IR absorption spectra for Chl-a_3 in the gas phase. The neutral (A), cation (B) and "cation minus neutral" (C) IR spectra are shown.

Table 3
Prominent harmonic vibrational mode frequencies (and intensities) along with proposed assignments for Chl-a_3, calculated using the B3LYP method and the 6-31G(d) basis

Modes	Chl-a_3 ν(I)	Chl-a_3^+ ν(I)
ν(13^1-keto C=O only)		1838(394)
ν(C=O) s	1817(339)	
ν(C=O) as	1806(563)	
ν(13^3-ester C=O only), δ(CH_3)		1804(228)
ν(C=C) vinyl	1701(2)	1684(59)
ν(C_{15}=C_{16}, C_{19}=C_{20})	1659(282)	
ν(C_{14}=C_{15}, C_{19}=C_{20}),		1639(344)
ν(C_2=C_3, C_{14}=C_{15}, N_{23}=C_{14})	1595(139)	
ν(C_{12}=C_{13}, C_{20}=C_1), δ(C–H)		1582(389)
ν(C_5=C_6, C_{15}=C_{16}), γ(C–H)		1567(396)

Frequencies have not been scaled. *Abbreviations:* ν, δ, γ, stretching, bending and rocking modes; as, antisymmetric; s, symmetric.

antisymmetric/symmetric vibrations of both C=O groups, respectively (Table 3). The antisymmetric stretching of both C=O modes is about 1.6 times higher in intensity than the symmetric mode (Table 3). Fig. 5 shows a view of the atomic motions of the C=O groups for the antisymmetric C=O mode of neutral Chl-a_3 at 1806 cm^{-1}.

Upon Chl-a_3^+ formation the C=O modes are clearly separated (Table 3). However, the highest frequency vibration at 1838 cm^{-1} is due to the 13^1-keto C=O group, while the mode at 1804 cm^{-1} is due to the 13^3-ester C=O group.

These calculated results for Chl-a_3 and Chl-a_3^+ disagree with experimental data. Firstly, for neutral Chl-*a* in THF, the 13^1-keto C=O mode is uncoupled from the 13^3-ester C=O mode [9,10]. Secondly, for Chl-a^+ in THF, the 13^1-keto C=O mode frequency is 33 cm^{-1} lower than that of the 13^3-ester C=O mode (1718 cm^{-1} versus 1751 cm^{-1}) [9]. Aside from the C=O modes, the frequencies of most of the other dominant modes of Chl-a_3 are very similar to that found for Chl-a_1 and Chl-a_2.

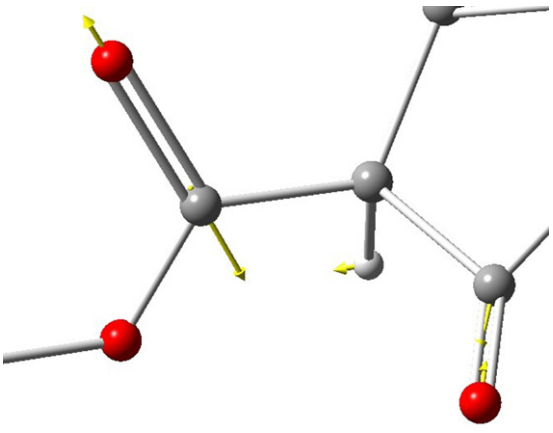

Fig. 5. Atomic displacements of the 1806 cm^{-1} vibrational modes of Chl-a_3 around ring V. The length of the arrows is representative of the magnitude of the movement of the atom upon vibration. For the optimized molecular configuration the 13^3 carboxymethyl group is out of the plane of the porphyrin ring.

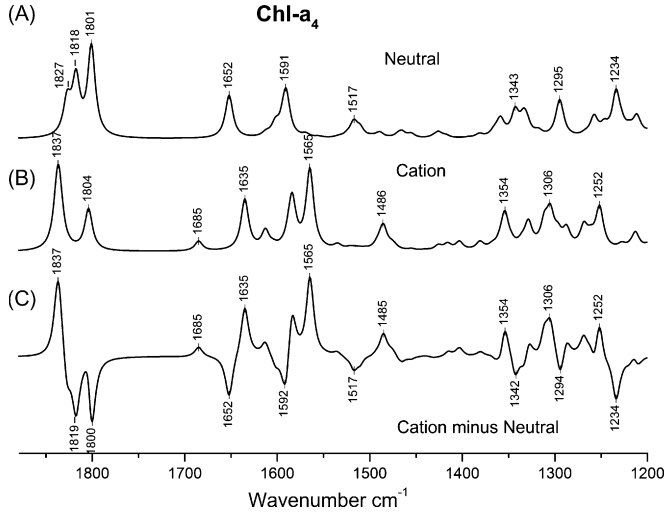

Fig. 6. Calculated IR absorption spectra for Chl-a_4 in the gas phase. The neutral (A), cation (B) and ''cation minus neutral'' (C) IR spectra are shown.

3.4. Calculation of the vibrational properties of Chl-a_4

A final set of calculations were undertaken using a model that contained all three C=O groups. This model, called Chl-a_4 (Fig. 2D) is most representative of Chl-*a*. Fig. 6 shows calculated absorbance spectra for (A) Chl-a_4 and (B) Chl-a_4^+. The ''cation minus neutral'' IR DS is also shown in Fig. 6C. Table 4 lists the C=O harmonic vibrational mode frequencies and intensities (in parenthesis) for Chl-a_4 and Chl-a_4^+. The complete set of calculated normal mode frequencies and intensities are presented in Supplementary information 4.

For Chl-a_4 the band at 1827 cm^{-1} is due only to the 17^3-ester C=O group. This mode up-shifts 8 cm^{-1} upon cation formation and changes little in intensity. This behavior is virtually the same as that found for the same mode of Chl-a_2. The 17^3-ester C=O group is therefore little affected by the presence of the 13^3-ester and the 13^1-keto C=O groups. As was found for Chl-a_3, the 13^1-keto and 13^3-ester C=O groups are strongly coupled, and unique vibrations of either C=O groups do not exist for the neutral state. As for Chl-a_3, the antisymmetric vibration of the ester and keto C=O groups is found to occur at a lower frequency than the symmetric vibration. The intensity ratio of the two modes is also very similar to that found for Chl-a_3. Clearly, the 17^3-ester C=O group plays no role in uncoupling the 13^1-keto and 13^3-ester C=O vibrations.

Table 4
Prominent C=O harmonic vibrational mode frequencies (and intensities) for Chl-a_4 and Chl-a_4^+ calculated using the B3LYP method and the 6-31G(d) basis

Mode	Chl-a_4 ν(I)	Chl-a_4^+ ν(I)
ν(17^3-ester C=O)	1827(211)	1835(230)
ν(13^1-keto C=O)		1838(337)
ν(13^1-keto and 13^3-ester C=O) s	1818(347)	
ν(13^1-keto and 13^3-ester C=O) as	1801(556)	
ν(13^3-ester C=O)		1804(258)

Frequencies have not been scaled. *Abbreviations:* ν, stretching vibration; as, antisymmetric; s, symmetric.

Table 5
Harmonic vibrational mode frequency calculations of Chl-a_3 undertaken using the B3LYP method with different basis sets

Mode assignment	6-31G(d)	6-31+G(d)	6-31G(df,p)
$\nu(13^1$-keto and 13^3-ester C=O) s	1817/339	1792/270	1813/415
$\nu(13^1$-keto and 13^3-ester C=O) as	1806/563	1776/864	1801/480
$\nu(C_{15}{=}C_{16}, C_{19}{=}C_{20})$	1659/282	1653/313	1654/286
$\nu(C_2{=}C_3, C_{14}{=}C_{15}, N_{23}{=}C_{14})$	1595/139	1589/157	1589/159

Calculated frequencies are unscaled. *Abbreviations:* ν, stretching vibration; as, antisymmetric; s, symmetric.

For Chl-a_4^+, the 13^1-keto C=O vibration is separated from the 13^3-ester C=O vibration. However, again, the 13^1-keto C=O group vibrates at a higher frequency compared to the 13^3-ester C=O group. So calculations for neither Chl-a_3 nor Chl-a_4 in the neutral or cation state agree with experimental data. It could be possible that the basis set used in our calculations is at too low a level to adequately model the vibrational properties of the C=O modes. To test this hypothesis, we have calculated the vibrational mode frequencies and intensities of Chl-a_3 using the 6-31+G(d) and the 6-31G(df,p) basis. Table 5 lists frequencies for the C=O and C=C modes of Chl-a_3 calculated using the three different basis sets.

For the C=C stretching vibrations the frequencies and intensities of the modes are similar for all three basis sets. However, the C=O modes are quite different. At the 6-31G(df,p) level the calculated frequencies for the antisymmetric/symmetric C=O modes are lowered only by 5/4 cm^{-1}, respectively. The intensity of the two C=O modes is calculated to be about the same as that found at the 6-31G(d) level. The calculations are therefore hardly improved at the 6-31G(df,p) level compared to the 6-31G(d) level.

At the 6-31G+(d) level, however, the vibrational frequencies of the antisymmetric/symmetric C=O modes decrease by 30/25 cm^{-1}, compared to that found at the 6-31G(d) level. In addition, at the 6-31+G(d) level, the antisymmetric C=O mode increases in intensity at the expense of the symmetric C=O mode. The antisymmetric C=O mode is dominated more by the 13^1-keto C=O vibration while the symmetric C=O mode is dominated more by the 13^3-ester C=O vibration.

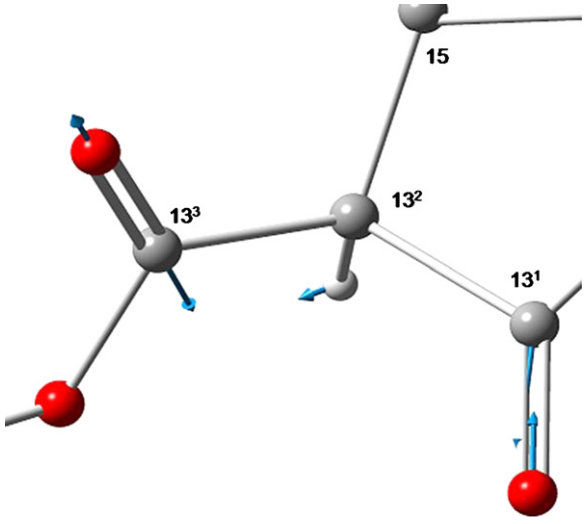

Fig. 7. Atomic displacements of the 1776 cm^{-1} vibrational modes of Chl-a_3 calculated at B3LYP/6-31+G(d) level. The length of the arrows is representative of the magnitude of the movement of the atom upon vibration. For the optimized molecular configuration the 13^3 carboxymethyl group is out of the plane of the porphrin ring.

Fig. 7 shows the atomic displacements that occur for antisymmetric C=O mode of Chl-a_4 at 1776 cm^{-1} (compare to Fig. 5). Thus, from the calculations at the 6-31+G(d) level, the trend appears to be towards a 13^1-keto C=O vibration at lower frequency than the 13^3-ester C=O vibration, with the 13^1-keto C=O vibration being more intense. These calculated observations are more in line with experimental observations. So calculations at the 6-31+G(d) level do appear to lead to a more accurate description of the vibrational properties of the C=O modes of Chl-*a*. However, even at the 6-31+G(d) level there is still considerable C=O mode coupling (Fig. 7), which is not observed experimentally. So the calculations at the 6-31+G(d) level lead to an improved but still inaccurate description of the C=O vibrational mode properties of Chl-*a*. The computational cost of these calculations, at the 6-31+G(d) level and above, prevents the widespread applicability of the methods used here. In addition it is not entirely clear if calculations at the 6-31+G(d) level are really required, or are appropriate, as we have yet to explore the effects of solvent and hydrogen bonding on the C=O vibrational mode properties of Chl-*a*. In a future publication we will explore how hydrogen bonding and solvent effects impact the vibrational properties of the C=O groups of Chl-*a* in calculations undertaken at the 6-31G(d) level. Once these calculations have been undertaken it should be apparent if a higher level basis set is required to model the vibrational properties of the C=O modes of Chl-*a*.

The calculations outlined above were all performed using the B3LYP functional. However, we have also calculated IR DS for Chl-a_1 and Chl-a_4 using the BLYP and BHLYP functionals. These data are presented in Supplementary information 5. In Supplementary information 5, we conclude that the B3LYP functional provides slightly superior results (at least in terms of vibrational modes of the neutral and cation states) to the BLYP functional, both of which are superior to the BHLYP functional.

Cation induced frequency shifts can be correlated with the occupancy of the frontier orbitals (HOMO/LUMO). Electron density contours of the HOMO for Chl-a_1 and Chl-a_4 are presented in Supplementary information 6. The HOMO we calculate for Chl-a_1 is very similar to that calculated previously [12]. We find that the HOMO's for the Chl-a_1 and Chl-a_4 models studied here are very similar (see Supplementary information 6). For the neutral/cation state the HOMO is doubly/singly occupied, and any cation induced frequency shifts can therefore be related to the electron density pattern of the HOMO. To a good approximation, the bonds in bonding/anti-bonding regions of the HOMO are weakened/strengthened upon cation formation, respectively. That is bonds in bonding/anti-bonding regions of the HOMO downshift/up-shift upon cation formation. For Chl-a_1, the HOMO is anti-bonding between the 13^1 carbon and the oxygen, and so an up-shift is observed for the C=O mode upon cation formation [12].

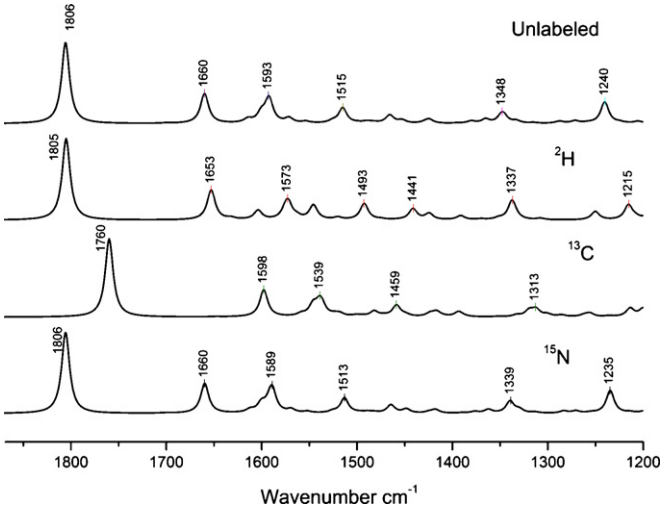

Fig. 8. Calculated IR absorbance spectra for neutral (top), ^{2}H, ^{13}C and ^{15}N labeled (bottom) Chl-a_1.

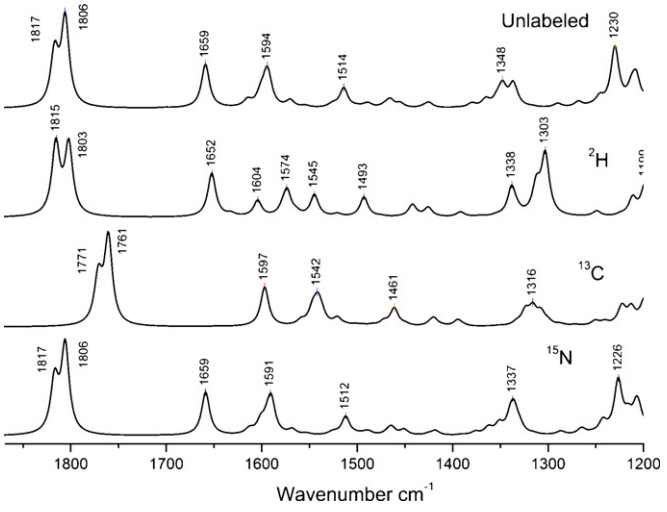

Fig. 9. Calculated IR absorbance spectra for neutral (top), ^{2}H, ^{13}C and ^{15}N labeled (bottom) Chl-a_3.

3.5. Calculated isotope-induced frequency shift for Chl-a_1 and Chl-a_3

Isotope induced band shifts provide a convenient way to characterize which molecular groups contribute to observed IR absorbance and absorbance difference bands. IR absorbance spectra for deuterated Chl-*a* have been obtained [10]. In addition, FTIR DS have been obtained for ^{13}C labeled Chl-*a* [24]. It is therefore of interest to see if our calculations can accurately calculate isotope induced band shifts for Chl-*a*. The above discussion indicates that many of the vibration modes are considerably mixed, with several types of molecular bonds contributing to the mode. Given the mixed nature of these modes it is not at all clear what frequency shifts might be expected upon isotope labeling. Figs. 8 and 9 show calculated absorbance spectra of unlabeled, ^{2}H, ^{13}C and ^{15}N labeled Chl-a_1 and Chl-a_3, in the 1800–1200 cm^{-1} region, respectively. Calculations undertaken for isotope labeled Chl-a_2 are essentially identical to that for Chl-a_1 (data not shown). Normal mode assignments, frequencies, intensities and frequency shifts for Chl-a_1 and Chl-a_3 are listed in Tables 6 and 7, respectively.

For Chl-a_1, the 13^1-keto C=O vibration at 1806 cm^{-1} is basically unaffected in both frequency and intensity by deuteration (Fig. 8 and Table 6). For Chl-a_3, however, the asymmetric vibration of both C=O groups is downshifted 4 cm^{-1} upon deuteration. The intensity of the mode is also decreased by ~20%. This deuteration effect most likely occurs via deuteration of the hydrogens near the 13^3-ester group, which is coupled to the keto C=O group. For deuterated Chl-*a* it

Table 6
Approximate mode assignments, frequencies and isotope induced frequency shifts for neutral Chl-a_1

Modes	Unlabeled	^{2}H		^{13}C		^{15}N	
	ν(I)	ν(I)	$\Delta\nu$	ν(I)	$\Delta\nu$	ν(I)	$\Delta\nu$
ν(13^1-keto C=O)	1806(716)	1805(720)	0.6	1760(686)	46	1806(718)	0
ν(C$_{15}$=C$_{16}$, C$_{19}$=C$_{20}$)	1660(264)	1653(265)	6.0	1598(239)	62	1660(263)	0
ν(C$_2$=C$_3$, C$_{12}$=C$_{13}$, N$_{23}$=C$_{14}$)	1593(157)	1573(141)	20	1539(115)	54	1589(202)	4
ν(C$_{12}$=C$_{13}$), δ(C–H)	1515(136)	1493(143)	22	1459(100)	56	1513(134)	2

Abbreviations: ν, δ, stretching, bending vibration.

Table 7
Approximate mode assignments, frequencies and isotope induced frequency shifts for neutral Chl-a_3

Modes	Unlabeled	^{2}H		^{13}C		^{15}N	
	ν(I)	ν(I)	$\Delta\nu$	ν(I)	$\Delta\nu$	ν(I)	$\Delta\nu$
ν(C=O) s	1817(339)	1816(459)	1	1771(300)	46	1817(338)	0
ν(C=O) as	1806(564)	1802(454)	4	1761(555)	45	1806(566)	0
ν(C$_{15}$=C$_{16}$, C$_{19}$=C$_{20}$)	1659(282)	1652(282)	7	1597(254)	62	1659(280)	0
ν(C$_2$=C$_3$, C$_{14}$=C$_{15}$, N$_{23}$=C$_{14}$)	1595(139)	1573(160)	22	1542(144)	53	1590(207)	5
ν(C$_{12}$=C$_{13}$, N$_{23}$=C$_{14}$) δ(C–H)	1514(113)	1545(140)	?	1461(115)	53	1512(114)	2

Abbreviations: ν, δ, stretching, bending vibration; as, antisymmetric; s, symmetric.

is found that the 13^3-ester C=O mode frequency downshifts 5 cm^{-1} upon deuteration while the 13^1-keto C=O mode frequency downshifts 3 cm^{-1} upon deuteration [25].

For Chl-a_1, the pure 13^1-keto C=O vibration downshifts 46 cm^{-1} upon ^{13}C labeling without much change in intensity of the mode. For Chl-a_3 the antisymmetric and symmetric C=O vibrations are downshifted 45-46 cm^{-1} upon ^{13}C labeling, again with little change in intensity of the modes. For ^{13}C labeled Chl-a and Chl-a^+ it is found that the 13^3-ester C=O mode frequency downshifts 42–43 cm^{-1} while the 13^1-keto C=O mode frequency is found to downshift 41–44 cm^{-1} [24]. In the simple harmonic oscillator approximation, a pure C=O mode at 1700 cm^{-1} is expected to downshift 37.8 cm^{-1} upon ^{13}C labeling. Thus, our calculated ^{13}C induced downshifts for the C=O modes of Chl-a_1 and Chl-a_3 agree well with that found experimentally.

For Chl-a_1 and Chl-a_3, the prominent C=C vibration at 1659–1660 cm^{-1} is calculated to downshifts 62 cm^{-1} upon ^{13}C labeling without much change in intensity of the mode. In the simple harmonic oscillator approximation, a pure C=C mode that vibrates at 1600 cm^{-1} is expected to downshift 62.8 cm^{-1} upon ^{13}C labeling. A downshift of ~60 cm^{-1} is also found for the negative band near 1609 cm^{-1} in ^{13}C labeled (Chl-a^+ minus Chl-a) FTIR DS [24]. The large difference in the downshifts found for C=C and C=O modes of Chl-a is a very useful feature that can be of high diagnostic value.

For Chl-a_1 and Chl-a_3 the C=O modes and the C=C modes above 1650 cm^{-1} are not affected by ^{15}N labeling. These modes are clearly uncoupled with the pyrrol nitrogen's. For many of the C=C vibrations below 1600 cm^{-1} there is a considerable ^{15}N induced effect, however.

4. Conclusions

DFT using the B3LYP method and the 6-31G(d) basis can be used to accurately model some of the vibrational properties of Chl-a and Chl-a^+ in polar solvent. This is especially true for the C=C modes. The isotope induced band shifts can also be accurately calculated.

DFT based calculations using the B3LYP method and the 6-31G(d) basis can be used to accurately calculate the cation minus neutral IR difference spectra for pyrochlorophyll-a. This is mainly because the 17^3-ester C=O is totally uncoupled from the 13^1-keto C=O group.

DFT based calculations using the B3LYP method and the 6-31G(d) basis do not accurately predict the nature of the cation minus neutral IR difference spectra for Chl-a. We are currently investigating if this is because the calculation is undertaken at too low a level, or whether solvent and electrostatic effects not considered in the calculation are important. Even using the computationally expensive 6-31G+(d) basis we cannot accurately simulate Chl-a infrared absorption spectra.

Acknowledgements

This work was supported by the National Research Initiative of the USDA Cooperative State Research Education and Extension Service grant number 2004-35318-14889, and NSF grant number DBI: 0352324 to G.H. R.W. was supported by a fellowship from the Molecular Basis of Disease Program at Georgia State University.

Appendix A. Supplementary data

Supplementary data associated with this article can be found, in the online version, at doi:10.1016/j.vibspec.2007.03.005.

References

[1] H. Scheer, Chlorophylls, CRC Press, Boca Raton, FL, 1991.
[2] J. Barber, The Photosystems: Structure, Function, and Molecular Biology, Elsevier Science Publishers, Amsterdam, New York, 1992.
[3] B. Ke, Photosynthesis: Photobiochemistry and Photobiophysics, Kluwer Academic Publishers, Dordrecht; Boston, 2001.
[4] R.E. Blankenship, Molecular Mechanisms of Photosynthesis, Blackwell Science, Oxford; Malden, MA, 2002.
[5] E. Nabedryk, in: H.H. Mantsch, D. Chapman (Eds.), Infrared Spectroscopy of Biomolecules, Wiley-Liss, New York, 1996 , pp. 39–81.
[6] W. Mäntele, in: J. Deisenhofer, J. Norris (Eds.), The Photosynthetic Reaction Center, Academic Press, San Diego, 1993, pp. 239–283.
[7] W. Mäntele, in: R.E. Blankenship, M.T. Madigan, C.E. Bauer (Eds.), Anoxygenic Photosynthetic Bacteria, Kluwer Academic Publishers, Dordrecht; Boston, 1995, pp. 627–647.
[8] W. Mäntele, E. Wollenweber, E. Nabedryk, J. Breton. Proc. Natl. Acad. Sci. U.S.A. 85 (1988) 8468–8472.
[9] E. Nabedryk, M. Leonhard, W. Mantele, J. Breton. Biochem. 29 (1990) 3242–3247.
[10] J.J. Katz, R.C. Dougherty, L. Boucher, in: L.P. Vernon, G.R. Seely (Eds.), The Chlorophylls, Academic Press, New York, 1966, pp. 185–251.
[11] S. Sinnecker, W. Koch, W. Lubitz, J. Phys. Chem. B 106 (2002) 5281–5288.
[12] P. O'Malley, J. Am. Chem. Soc. 122 (2000) 7798–7801.
[13] Y. Sun, H. Wang, F. Zhao, J. Sun, Chem. Phys. Lett. 387 (2004) 12–16.
[14] M. Ceccarelli, M. Lutz, M. Marchi, J. Am. Chem. Soc. 122 (2000) 3532–3533.
[15] V.V. Nechaev, K.V. Berezin, Opt. Spectrosc. 96 (2004) 217–220.
[16] K.V. Berezin, V.V. Nechaev, O.D. Ziganshina, J. Struct. Chem. 45 (2004) 217–224.
[17] K. Bandaranayake, V. Sivakumar, R. Wang, G. Hastings, Vib. Spectrosc. 42 (2006) 78–87.
[18] M.J. Frisch, G.W. Trucks, H.B. Schlegel, G.E. Scuseria, M.A. Robb, J.R. Cheeseman, J.A. Montgomery Jr., T. Vreven, K.N. Kudin, J.C. Burant, J.M. Millam, S.S. Iyengar, J. Tomasi, V. Barone, B. Mennucci, M. Cossi, G. Scalmani, N. Rega, G.A. Petersson, H. Nakatsuji, M. Hada, M. Ehara, K. Toyota, R. Fukuda, J. Hasegawa, M. Ishida, T. Nakajima, Y. Honda, O. Kitao, H. Nakai, M. Klene, X. Li, J.E. Knox, H.P. Hratchian, J.B. Cross, V. Bakken, C. Adamo, J. Jaramillo, R. Gomperts, R.E. Stratmann, O. Yazyev, A.J. Austin, R. Cammi, C. Pomelli, J.W. Ochterski, P.Y. Ayala, K. Morokuma, G.A. Voth, P. Salvador, J.J. Dannenberg, V.G. Zakrzewski, S. Dapprich, A.D. Daniels, M.C. Strain, O. Farkas, D.K. Malick, A.D. Rabuck, K. Raghavachari, J.B. Foresman, J.V. Ortiz, Q. Cui, A.G. Baboul, S. Clifford, J. Cioslowski, B.B. Stefanov, G. Liu, A. Liashenko, P. Piskorz, I. Komaromi, R.L. Martin, D.J. Fox, T. Keith, M.A. Al-Laham, C.Y. Peng, A. Nanayakkara, M. Challacombe, P.M.W. Gill, B. Johnson, W. Chen, M.W. Wong, C. Gonzalez, J.A. Pople, Gaussian 03, Revision C.02 (2004).
[19] R.A. Wheeler, L.A. Eriksson (Eds.), Theoretical Biochemistry-Processes and Properties of Biological Systems, Elsevier, 2001 , pp. 655–690.
[20] BandaranayakeF K.M.P., R. Wang, G. Hastings, Biochemistry 45 (2006) 4121–4127.
[21] G. Rauhut, P. Pulay, J. Phys. Chem. 99 (1995) 3093–3100.

[22] R. Heald, T. Cotton, J. Phys. Chem. 94 (1990) 3968–3975.
[23] M. Lutz, W. Mantele, in: H. Sheer (Ed.), Chlorophylls, CRC Press, Boca Raton, 1991, pp. 855–902.
[24] B.A. Tavitian, E. Nabedryk, A. Wollenweber, W. Mantele, J. Breton, in: E. Schmid, F. Schneider, F. Siebert (Eds.), Spectroscopy of Biological Molecules-New Advances, Wiley and Sons, Chichester, UK, 1988, pp. 297–300.
[25] J. Breton, E. Nabedryk, W. Leibl, Biochemistry 38 (1999) 11585–11592.
[26] M.G. Muller, J. Niklas, W. Lubitz, A.R. Holzwarth, Biophys. J. 85 (2003) 3899–3922.